Frequency of Persistent Blocking and Ridge Events Related to Precipitation over Eastern China during August and Its Preceding Atmospheric Signals

BO ZHANG

National Meteorological Center, China Meteorological Administration, Beijing, China

GE LIU

State Key Laboratory of Severe Weather, Chinese Academy of Meteorological Sciences, Beijing, and Collaborative Innovation Centre on Forecast and Evaluation of Meteorological Disasters, Nanjing University of Information Science and Technology, Nanjing, China

YUEJIAN ZHU

Environmental Modeling Center, NOAA/NWS/NCEP, College Park, Maryland

NING SHI

Collaborative Innovation Centre on Forecast and Evaluation of Meteorological Disasters, Nanjing University of Information Science and Technology, Nanjing, China

(Manuscript received 5 March 2019, in final form 21 August 2019)

ABSTRACT

Based on a recently developed approach that can recognize both persistent blocking and ridge events effectively, the contributions of the frequency of these persistent events (FOPE) over different regions in Eurasia to precipitation over eastern China were investigated. The results reveal that, the FOPE over the longitudinal range of 110°–130°E, near the Stanovoy Mountains and the Okhotsk Sea, is significantly correlated with precipitation over the middle and lower reaches of the Yangtze River (MLRYR) during summer, particularly in August. The preceding full July (or 1–20 July) mean Balkhash Lake–Caucasus geopotential height index, which measures the combined effect of the Balkhash Lake and Caucasus geopotential height anomalies, is closely related to the August geopotential height anomaly around the Stanovoy Mountains and the Okhotsk Sea, and can therefore reflect the August 110°–130°E FOPE. The predictability based on this preceding atmospheric signal seems to be attributable to slow-varying atmospheric processes on a subseasonal (20-day mean) time scale. On this time scale, the Balkhash Lake and Caucasus geopotential height anomalies occur prior to, and seem to modulate, the geopotential height anomaly around the Stanovoy Mountains and the associated 110°–130°E FOPE through an eastward extension and through exciting a positive–negative–positive pattern in 500-hPa geopotential heights, respectively. As a result of the slow-varying atmospheric processes, this preceding atmospheric signal performs well in predicting the August 110°–130°E FOPE, which also facilitates the prediction of the MLRYR precipitation.

1. Introduction

As one of the most densely populated and economically developed areas in China, the middle and lower reaches of the Yangtze River (MLRYR) are an important area in terms of the country's ecological and economic sustainable development (Zhang et al. 2008). However, this area experiences frequent floods, directly attributable to the abnormally high precipitation that often occurs during summer over the MLRYR (Yin and Li 2001). For instance, in the summer of 1998, a severe flood struck the MLRYR, causing a death toll of more than 3000 and direct economic losses of 250 billion Chinese Yuan (Zhang et al. 2001; Ding and Hu 2003). More recently, in 2017, the Changjiang Water Resources Commission of the Ministry of Water Resources

Corresponding author: Ge Liu, liuge@cma.gov.cn

DOI: 10.1175/WAF-D-19-0047.1

reported that, as a direct result of the high precipitation and associated flooding in the MLRYR, the death toll was around 2000 and there were economic losses totaling 93.9 billion Chinese Yuan. Therefore, it is essential to investigate the potential mechanisms of anomalous precipitation over the MLRYR during summer.

In terms of the monthly variability in summer, the main rain belt appears to the south of the Yangtze River in June, over the MLRYR in July, and over southern coast of China in August, which constitutes a typical evolution of the rain belt during summer (Wang and Ding 2008). However, such a typical evolution may change in certain years. For example, in 1980, the main rain belt stayed over the MLRYR for a longer time than normal, with anomalously high local precipitation during August (Zhao 1999). In fact, such a process is not as rare as one might expect. Indeed, according to results based on an expanded empirical orthogonal function (Chen et al. 2007), it was concluded that this kind of process should be considered as one of the most dominant modes reflecting the rain belt's evolution during summer. Clearly, it is necessary to further explore how atmospheric circulation systems modulate precipitation over the MLRYR during the whole summer, and during each month of the summer season.

Blocking is one of the most important atmospheric circulation systems at middle and high latitudes, contributing to weather anomalies over different regions during different seasons, such as large-range cold waves (Cattiaus et al. 2010; Buehler et al. 2011; Pfahl and Wernli 2012; Ye et al. 2015; Brunner et al. 2017) and heatwaves (Dole et al. 2011; Matsueda 2011; Hoskins and Woollings 2015; Horton et al. 2016). The maintenance of Eurasian blocking highs also plays an important role in adjusting large-scale droughts and floods over several areas of China (Bi and Ding 1992; Wu et al. 1994; Zhang and Tao 1998; Lu and Huang 1999; Yu and Lin 2006; Gu et al. 2016), including the MLRYR region (Sun and Zhao 2003; Shen et al. 2008). Besides blockings, it is known that open ridges can cause high-impact weather anomalies in certain cases, such as the extreme heatwave in early August 2003 over Europe (Black et al. 2004) and an extreme cold event in East Asia (Bueh and Xie 2015). The accumulative effect of multiple blockings and/or open ridges may even adjust seasonal mean temperature and precipitation anomalies. For instance, the summer-mean high pressure (anticyclone) anomaly over the Okhotsk Sea, which should be considered as a common outcome of both blockings and open ridges, is conducive to higher-than-normal precipitation and associated flooding over the MLRYR (Zhang and Tao 1998).

The abovementioned studies show the importance of blockings and open ridges in affecting temperature and precipitation anomalies on different time scales, including the summer precipitation anomaly over the MLRYR. Many methods have been developed to identify closed or nonclosed blockings (Kaas and Branstator 1993; Pelly and Hoskins 2003; Renwick 2005; Barriopedro et al. 2006; Barnes et al. 2012; Small et al. 2014; Faranda et al. 2016; Parsons et al. 2016; Martineau et al. 2017; Liu et al. 2018). Of these methods, a Lagrangian objective approach recently developed by Liu et al. (2018) was used in the present study. This approach can effectively identify and track persistent open ridges of 500-hPa geopotential height (Z500), either as an individual event or as a part attached to a blocking anticyclone, in turn successfully capturing the formation and movement of open ridges and closed blockings (Liu et al. 2018). This method is suitable for our study that focuses on the common effect of both blockings and open ridges on the MLRYR precipitation. As such, we used it to recognize persistent open ridges and blocking highs (maxima) of Z500, which we abbreviate as PMZ.

The summer precipitation anomaly over the MLRYR is closely linked to variations in the East Asian summer monsoon that are primarily driven or affected by many large-scale land–sea–atmosphere slow-varying factors, such as El Niño–Southern Oscillation (ENSO; e.g., Wang et al. 2000; Wang et al. 2009a; Zhang et al. 2016a,b), sea surface temperature anomalies in the North Pacific (Guo et al. 2017) and the North Atlantic Ocean (Guo et al. 2017), Arctic sea ice anomalies (Wu et al. 2004), North Atlantic Oscillation (Wu et al. 2009), Arctic Oscillation (Gong et al. 2011), and Antarctic Oscillation (Fan 2006). These slow-varying factors provide precursory signals for the prediction of summer precipitation over the MLRYR. Dynamic prediction based on numerical climate models has achieved great success in terms of the seasonal prediction of tropical sea surface temperatures, ENSO, and low-latitude atmospheric circulation (Zhou and Zeng 2001; Zhu et al. 2013; Saha et al. 2014). However, the prediction skill of dynamical models is still quite poor for the East Asian summer monsoon–related precipitation (e.g., the MLRYR precipitation) in extratropical regions (Wang et al. 2009b).

A successful prediction for the frequency of PMZ events (FOPE; see definition in section 2) over mid- and high-latitude regions may be helpful for the prediction of summer precipitation over the MLRYR, since blockings and open ridges, as well as their common and accumulative effects, seem to modulate the MLRYR precipitation during summer. Nevertheless, a

recent study on the forecasts by the NCEP Global Ensemble Forecast System showed that the skill score associated with the FOPE is generally lower in the Euro–Atlantic–Asia sector (He et al. 2019). To provide an additional tool or guidance to predict the FOPE in a specific region, we further explored preceding atmospheric signals through statistical analyses, which may also help to improve the prediction of the MLRYR precipitation.

Given the importance of the MLRYR precipitation and the associated contribution of blocking and open ridges, this study focused on the relationships between the precipitation over eastern China and the FOPE over different regions, which can disclose the location of the crucial region of the PMZ events influencing precipitation over eastern China. The preceding atmospheric signals of the FOPE over this crucial region were also investigated, which is, to some extent, favorable for understanding and improving the prediction of precipitation over eastern China.

The rest of this paper is organized as follows: section 2 describes the data and methods. Section 3 examines the relationship between the FOPE and the precipitation over eastern China during summer. Section 4 investigates the preceding atmospheric signals of the FOPE. A possible interpretation that partly explains the delayed impact of the preceding signals is also proposed in section 4. Finally, a summary and discussion are provided in section 5.

2. Data and methods

a. Data

Following Liu et al. (2018), we used the daily Z500 with a spatial resolution of 2.5° × 2.5° to identify PMZ events. The data were obtained from the NCEP–NCAR reanalysis dataset (Kalnay et al. 1996). The NCEP monthly pressure-level geopotential height and U and V winds (Kalnay et al. 1996) and the monthly precipitation on 2.5° × 2.5° grids from the Climate Prediction Center Merged Analysis of Precipitation (CMAP; Xie and Arkin 1997) were also used in this study. The above datasets were extracted for the period 1979–2017.

b. Definition of PMZ and FOPE

With reference to Liu et al. (2018), a PMZ event was identified when its core included a local eddy anomaly maximum (Z^*) of Z500 and the neighboring grid points had values greater than 100 geopotential meters (gpm) and decreased radially to about 20 gpm smaller than the maximum value. If two cores shared at least one grid point and moved at a speed of no greater than 10° of longitude per day on consecutive Z^* maps, the two cores were taken to belong to the same PMZ event. A PMZ event should persist for two days or longer; otherwise, it cannot be regarded as a PMZ event. To exclude weak ridges, each of the tracked cores was expanded to contain more contiguous points whose Z^* values decreased radially to about 100 gpm.

The FOPE was defined as follows: If a PMZ event appeared (including its occurrence or passing through) over a grid point in a day, one time/day was counted for this grid point. If a persistent PMZ event occupied a grid point for n days, n times/days were counted for this grid point. If a PMZ event disappeared or left this grid point and another PMZ event occurred or came to govern this grid point, we needed to add up more times/days for the latter PMZ event. Here, the frequency for times/days was essentially the accumulative duration governed by persistent PMZ events at a grid point. The FOPE over a region could be calculated by averaging the times/days at each grid point within the region. As such, the regional-mean FOPE reflected the duration (times/days) when PMZ events governed the region.

c. Statistical analysis methods

In this study, the region (27.5°–33°N, 107°–123°E; see black box in Fig. 2) was referred to as the MLRYR region. The MLRYR precipitation index was defined as the regional mean of precipitation over the MLRYR region.

Correlation, composite, and regression analysis were used in this study to examine the relationship between the FOPE and the MLRYR precipitation. The variation of a variable is often related to multiple factors. Thus, a linear fitting method was applied to decompose the independent effect of one factor from that of another (Hu et al. 2012). For two time series X_1 and X_2, the X_2-related variation (called X_1') of X_1 can be obtained through a linear fitting method, in which the variation of X_1 is regarded as a dependent variable and the variation of X_2 as an independent variable. The residual of the linear fitting (i.e., the difference X_1 minus X_1') can be used to reflect the individual variation of X_1 independent of X_2. Using this method (Hu et al. 2012), we investigated the individual effects of the preceding atmospheric signals over several crucial regions on the FOPE. In the present study, unless otherwise stated, the Student's t test was employed to evaluate the statistical significance of these analyses.

3. Relationship between the FOPE and precipitation over eastern China

a. Climatological distribution of the FOPE

Before exploring the relationship between the FOPE and precipitation over eastern China during summer (June, July, and August), we first detected the climatological

summer mean distribution of the FOPE during the period 1979–2017 (Fig. 1). The area with a FOPE ≥ 5 days during summer extends eastward from Europe to eastern Russia, to the north of the Okhotsk Sea (around the longitude of 145°E; Fig. 1), whereas that during the other three seasons (spring, autumn and winter) extends only to the west of Lake Baikal (not shown).

The higher FOPE around the Okhotsk Sea reflects a longer-term control of blockings and ridges over this region, which often facilitate high precipitation over the MLRYR during summer (Sun and Zhao 2003; Shen et al. 2008). This motivated us to further investigate the relationship between the FOPE and precipitation over eastern China during summer. In particular, we sought to reveal the relationship between the FOPE over different longitudinal ranges in Eurasia and the MLRYR precipitation during summer. The PMZ events primarily appear between 50° and 80°N in Eurasia (Fig. 1). The latitudinal range of the FOPE is not specifically confined—that is, all PMZ events over Eurasia were included in our analyses.

b. *Relationship between the FOPE and MLRYR precipitation*

Correlation analysis showed that the summer FOPE over the region between 110° and 130°E (hereafter referred to as 110°–130°E FOPE) is significantly and positively correlated with simultaneous precipitation over the MLRYR region (black box in Fig. 2a). To investigate the relationship between the FOPE over different longitudinal ranges in Eurasia and the MLRYR precipitation, we also calculated the 5°-longitude sliding correlation coefficient between an MLRYR precipitation index and the FOPE over the regions from 30°–50°E to 130°–150°E (Fig. 3a). The results showed that the correlation coefficient between the FOPE over the 110°–130°E region and the MLRYR precipitation is highest (0.56) during summer, and is statistically significant at the 99.9% confidence level (Fig. 3a). In other words, the 110°–130°E region is the most crucial region where the FOPE is closely related to the MLRYR precipitation during summer.

The typical monthly evolution of the rain belt over southern China in summer can sometimes be altered by atmospheric circulation anomalies (Zhao 1999; Chen et al. 2007). To help understand the modulation of the rain belt by the FOPE anomaly, we further explored the relationship between the 110°–130°E FOPE and precipitation over eastern China during each month of the summer. The correlations between the 110° and 130°E FOPE and precipitation over eastern China during June, July, and August are shown in Figs. 2b–d, respectively. A significant positive correlation appears over the

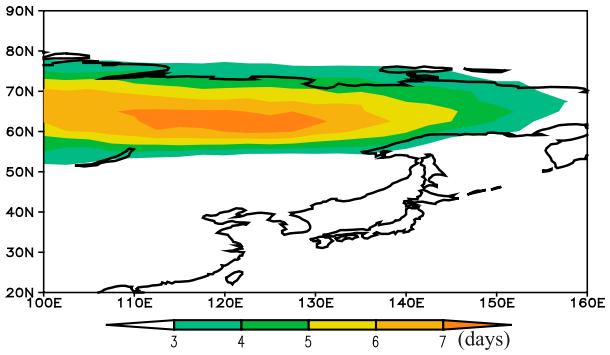

FIG. 1. Climatological mean (1979–2017) distribution of the summer (June, July, and August) frequency of persistent blocking and ridge events (FOPE; days).

MLRYR during August (Fig. 2d), which is in good agreement with that during summer (Fig. 2a). The 5°-longitude sliding correlation in August (Fig. 3b) also shows that the correlation coefficient between the MLRYR precipitation and the FOPE over 110°–130°E is the highest, consistent with the correlation result during summer (Fig. 3a). These results reveal that significant correlation between the 110°–130°E FOPE and the MLRYR precipitation can be found primarily in August, rather than in June and July. In other words, the close relationship between the 110°–130°E FOPE and the MLRYR precipitation during summer is mainly due to the high correlation between the two variables in August. As such, hereafter, the August 110°–130°E FOPE and simultaneous MLRYR precipitation are the main point of discussion.

Figure 4 shows the time series of the August 110°–130°E FOPE (red line) and simultaneous MLRYR precipitation (blue line) indices. These two indices show a similar variability, with a correlation coefficient of 0.57, significant at the 99.9% confidence level.

To further illustrate the anomalous precipitation over eastern China corresponding to a higher and lower 110°–130°E FOPE, we performed composite analyses. First, nine years (1980, 1988, 1991, 1998, 1999, 2000, 2011, 2015, and 2017) with a 110°–130°E FOPE ≥ 9 days (accounting for approximately 30% of all 31 days in August) were selected to composite the anomalous precipitation over eastern China in August (Fig. 5a). This composite result showed that significant positive precipitation anomalies appear over the MLRYR region, with a center of ≥40 mm over the lower reaches of the Yangtze River. Second, six years (1985, 1986, 1997, 2003, 2012 and 2016) with a 110°–130°E FOPE ≤ 2 days were selected to composite the anomalous precipitation over eastern China during August (Fig. 5b). This figure shows significant negative precipitation

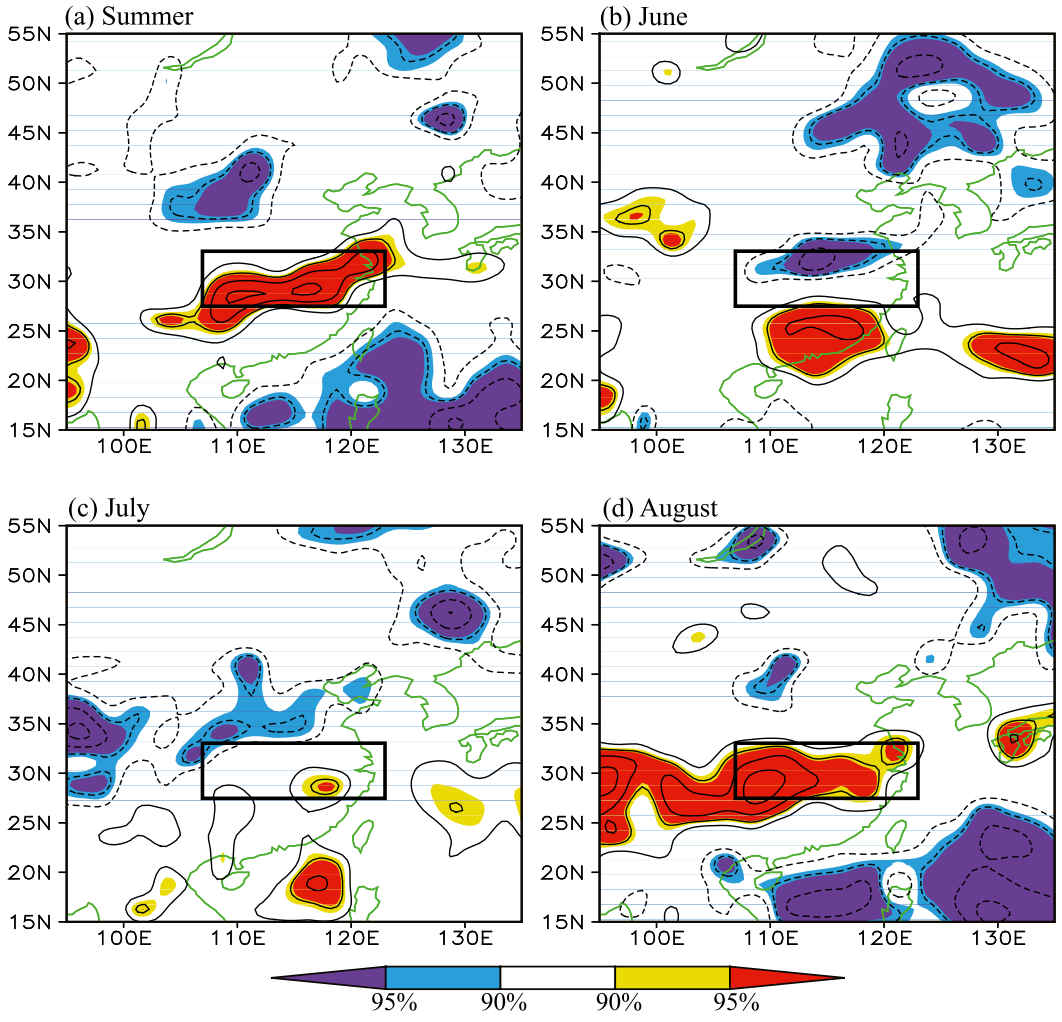

FIG. 2. (a) Distribution of correlation coefficients between the summer 110°–130°E FOPE and simultaneous precipitation over eastern China during 1979–2017. (b)–(d) As in (a), but for June, July, and August, respectively. Contours are drawn every 0.1 from the beginning contours of ±0.2. As shown in the color bar, yellow (red) shading denotes positive correlations significant at the 90% (95%) confidence level, and blue (purple) shading indicates negative correlations significant at the 90% (95%) confidence level. The black box represents the MLRYR region.

anomalies appearing over the MLRYR region, with a center of ≤−60 mm over the middle reaches, and one of ≤−40 mm over the lower reaches, of the Yangtze River. These two composites further indicate that, corresponding to a higher (lower) FOPE over the 110°–130°E region during August, a higher (lower) precipitation anomaly appears over the MLRYR at the same time.

In short, the aforementioned results signify that, of all PMZ events over Eurasia, those over the 110°–130°E region seem to play the most important role in terms of the relationship with the MLRYR precipitation during summer, particularly in August. Next, the large-scale atmospheric circulation anomalies associated with the 110°–130°E FOPE and the effects of these circulation anomalies on the MLRYR precipitation are discussed.

c. *Large-scale atmospheric circulation anomalies*

First, we present the atmospheric circulation anomalies associated with the MLRYR precipitation index (Figs. 6a,b). During August, the Z500 anomalies regressed upon the MLRYR precipitation index (Fig. 6a) shows an East Asian–Pacific (EAP) teleconnection pattern (Huang and Sun 1992; Lu 2004). With respect to Z500, this pattern is characterized by a positive anomaly at mid–high latitudes (around 45°–65°N), around the Stanovoy Mountains and the Okhotsk Sea, a negative anomaly at midlatitudes (around 30°–40°N) in East Asia, and a positive anomaly at low

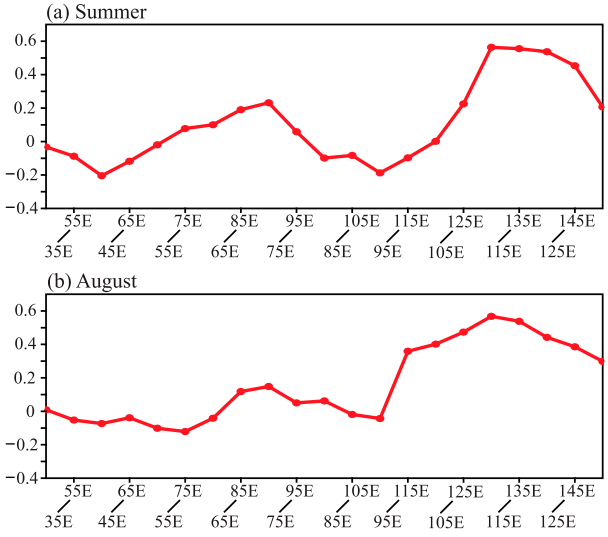

FIG. 3. The 5°-longitude sliding correlation coefficient between the MLRYR precipitation and the FOPE from the 30°–50°E to 130°–150°E regions during (a) summer and (b) August for the period 1979–2017.

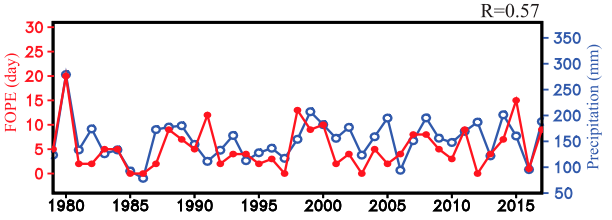

FIG. 4. Time series of the August 110°–130°E FOPE (red line; days) and simultaneous MLRYR precipitation (blue line; mm) indices during 1979–2017. The correlation coefficient between the two indices is 0.57, significant at the 99.9% confidence level.

latitudes, over the subtropical northwestern Pacific (Bueh et al. 2008; Shi et al. 2009). This is also a typical pattern contributing to higher precipitation over the MLRYR. Accompanying the positive geopotential height anomaly at mid–high latitudes, an anomalous 850-hPa anticyclone appears around the Stanovoy Mountains, inducing anomalous northeastward cold flow along the southeastern flank of this anomalous anticyclone (Fig. 6b). Moreover, the positive geopotential height anomaly at low latitudes reflects a stronger and farther-southward western Pacific subtropical high. Correspondingly, an anomalous 850-hPa anticyclone occurs over the subtropical northwestern Pacific, inducing anomalous southwestward warm flow to the MLRYR along the northwestern flank of this anomalous anticyclone (Fig. 6b). The anomalous cold and warm flows meet and hence facilitate higher precipitation over the MLRYR region.

The formation of the EAP pattern can be partly attributed to the meridional propagation of quasi-stationary Rossby waves, which are triggered by anomalous convective activity in the western Pacific warm pool (Nitta 1987; Huang and Sun 1992). A Rossby wave packet over high- and midlatitude Eurasia propagates toward East Asia in the upper troposphere and plays an important role in forming the mid–high- and midlatitude anomalies of the EAP pattern—that is, the EAP pattern results from interaction between high- and low-latitude circulation systems (Bueh et al. 2008; Shi et al. 2009).

According to the latter theory (Bueh et al. 2008; Shi et al. 2009), those PMZ events that frequently appear over the 110°–130°E region and are measured by the 110°–130°E FOPE, may at least partly be responsible for the mid–high- and midlatitude geopotential height anomalies of the EAP pattern. To verify this speculation, we studied the relationship between the 110°–130°E FOPE and atmospheric circulation anomalies.

As shown in Fig. 6c, the Z500 anomalies regressed upon the 110°–130°E FOPE also bear an EAP-like pattern, with a stronger and more significant positive anomaly around the Stanovoy Mountains and the Okhotsk Sea, centered at (55°N, 130°E). This implies that a higher (lower) 110°–130°E FOPE is an effective representation of the mid–high-latitude blockings and ridges appearing more (less) frequently and controlling the region around the Stanovoy Mountains and the Okhotsk Sea during August, and accordingly dominating the monthly mean geopotential height anomaly over this region.

Corresponding to the EAP-like pattern associated with the higher 110°–130°E FOPE (Fig. 6c), the anomalous 850-hPa winds over the East Asian coast (Fig. 6d) are also similar to those modulating the MLRYR precipitation (Fig. 6b), with an anomalous cold northeasterly flow and an anomalous warm southwesterly flow converging over the MLRYR region (Fig. 6d). The convergence between the anomalous cold and warm flows is favorable for higher MLRYR precipitation. On the contrary, the MLRYR region experiences lower precipitation in correspondence to a lower 110°–130°E FOPE. Therefore, the variability of MLRYR precipitation is closely related to that of 110°–130°E FOPE during August, via the modulation of the EAP pattern by the 110°–130°E FOPE.

It should be noted that, although there is a 110°–130°E FOPE-related positive anomaly over the subtropical northwestern Pacific (Fig. 6c), it is hard to declare that PMZ events stimulate such an anomaly according to current theories (Bueh et al. 2008; Shi et al. 2009). However, after removing the variability of the geopotential height averaged over the subtropical northwestern Pacific (15°–25°N, 115°–140°E) using the method of

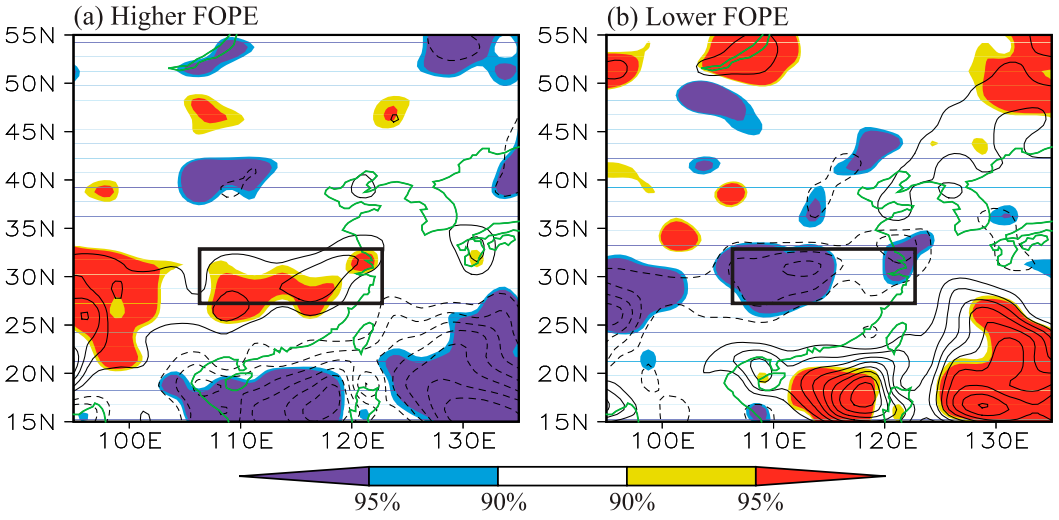

FIG. 5. Composites of August precipitation anomalies (mm) for the years with an August (a) higher and (b) lower FOPE. Contours are drawn every 20 mm from the beginning contours of ±20 mm. As shown in the colorbar, yellow (red) shading denotes positive precipitation anomalies significant at the 90% (95%) confidence level, and blue (purple) shading indicates negative precipitation anomalies significant at the 90% (95%) confidence level. The black box represents the MLRYR region.

linear fitting (Hu et al. 2012), the individual variability of the 110°–130°E FOPE is still closely related to the mid–high- and midlatitude anomalies of the EAP pattern (Fig. 7a) and is therefore intimately linked with the precipitation over the MLRYR region (Fig. 7b). The correlation coefficient between the individual variability of the 110°–130°E FOPE and MLRYR precipitation indices is 0.42, significant at the 99% confidence level. These results further support the notion that the development of the negative geopotential height

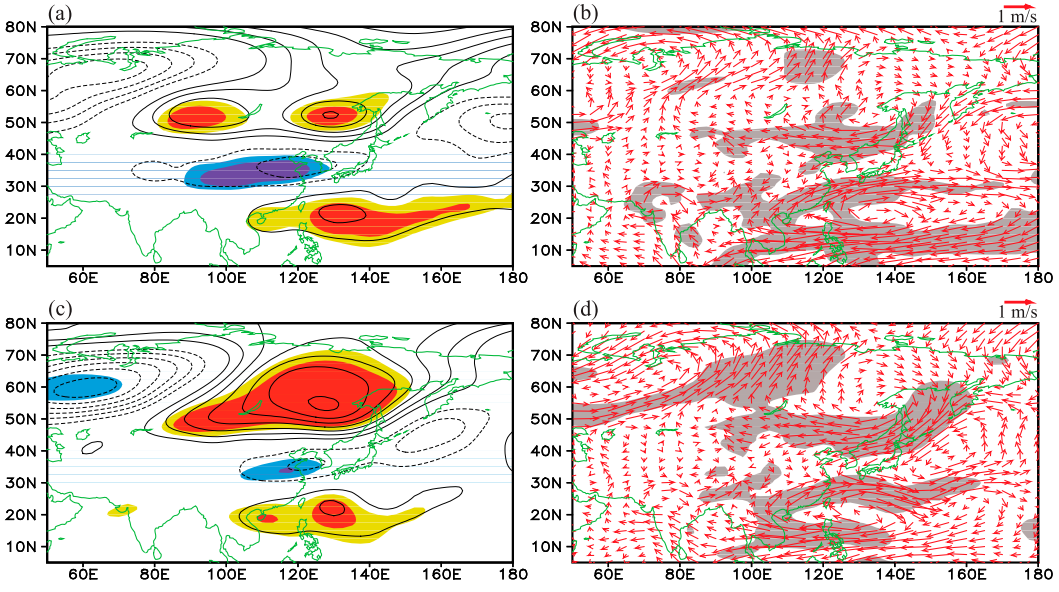

FIG. 6. Anomalous August (a) 500-hPa geopotential height (gpm) and (b) 850-hPa winds (m s^{-1}) regressed upon the simultaneous MLRYR precipitation index for the period 1979–2017. (c),(d) As in (a) and (b), respectively, but for the regression upon the 110°–130°E FOPE. In (a) and (c), contours are drawn every 3 gpm from the beginning contours of ±3 gpm. Yellow (red) shading denotes positive geopotential height anomalies significant at the 95% (99%) confidence level, and blue (purple) shading indicates negative geopotential height anomalies significant at the 95% (99%) confidence level. In (b) and (d), gray shading denotes anomalous winds significant at the 95% confidence level.

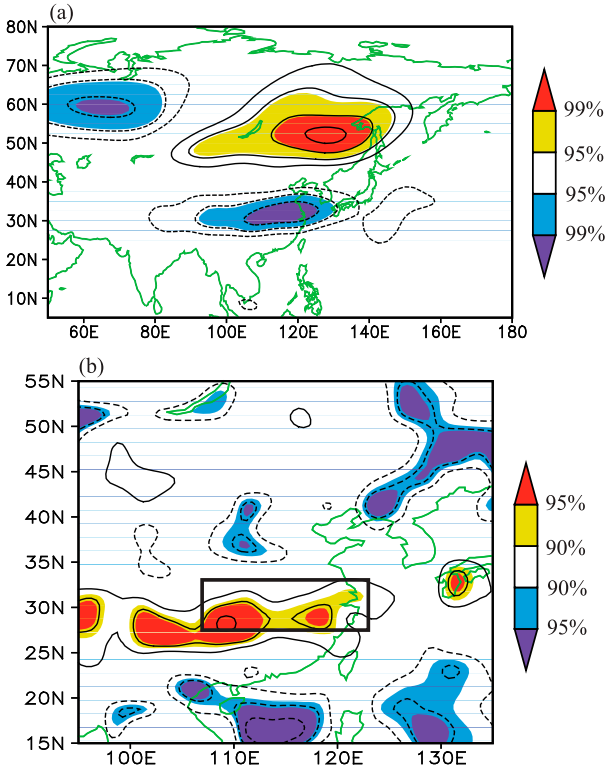

FIG. 7. Distribution of the correlation coefficients of (a) 500-hPa geopotential heights and (b) precipitation with the individual 110°–130°E FOPE index after removing the variability of the geopotential height averaged over the subtropical northwestern Pacific during August for the period 1979–2017. As shown in the colorbar in (a), yellow (red) shading denotes positive correlation significant at the 95% (99%) confidence level, and blue (purple) shading indicates negative correlation significant at the 95% (99%). In (b), the shading also denotes the significance of correlation, but for the 90% (95%) confidence level. In both (a) and (b), contours are drawn every 0.1 from the beginning contours of ±0.2.

anomaly over midlatitude East Asia partly emanates from Rossby wave energy dispersion of the positive geopotential height anomaly near the Okhotsk Sea (Shi et al. 2009), and meanwhile imply that the above process seems to be strongly related to the variability of the 110°–130°E FOPE.

In contrast, after removing the variability of the 110°–130°E FOPE, the individual variability of the low-latitude geopotential height anomaly over the subtropical northwestern Pacific is no longer closely related to the MLRYR precipitation (not shown), with a nonsignificant correlation coefficient of 0.23.

These results reveal that the variability of the 110°–130°E FOPE is undoubtedly important in exciting an EAP pattern and in turn modulating precipitation over the MLRYR during August. Therefore, it is also essential to investigate whether the August 110°–130°E FOPE can successfully be predicted through

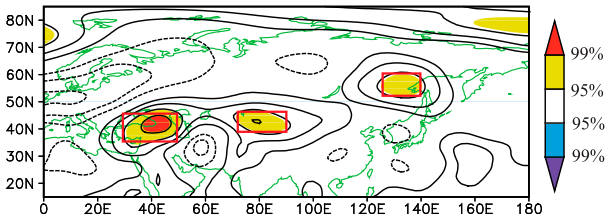

FIG. 8. Distribution of correlation coefficients between the August 110°–130°E FOPE and previous July 500-hPa geopotential heights during 1979–2017. Contours are drawn every 0.1 from the beginning contours of ±0.1. As indicated by the colorbar, yellow (red) shading denotes positive correlations significant at the 95% (99%) confidence level, and blue (purple) shading indicates negative correlation significant at the 95% (99%). The three red boxes from right to left denote the Stanovoy Mountains, Balkhash Lake, and Caucasus regions.

exploring precursory atmospheric signals using statistical analyses.

4. Preceding atmospheric signals of the 110°–130°E FOPE

The correlation between the August 110°–130°E FOPE index and previous July Z500 shows that there are three areas of significant positive correlations—namely, near the Stanovoy Mountains, Lake Balkhash, and the Caucasus (i.e., the three black boxes from right to left in Fig. 8). The preceding signals reflected by these significant correlations generally appear over the Stanovoy Mountains and to their west at midlatitudes, implying that the August 110°–130°E FOPE can possibly be tracked to upstream atmospheric circulation anomalies during the previous July. Correlation analysis further revealed that no significant correlations can be detected at midlatitudes during the earlier month (i.e., June; not shown). The results imply that the July atmospheric circulation anomalies at midlatitudes are useful in statistically predicting the August 110°–130°E FOPE, but the earlier (June) ones are not.

Based on Fig. 8, the regional averages of Z500 over the Stanovoy Mountains (52°–60°N, 126°–140°E; the red box on the right in Fig. 8), Lake Balkhash (39°–46°N, 72°–90°E; the red box in the middle in Fig. 8) and the Caucasus (36°–46°N, 30°–50°E; the red box on the left in Fig. 8) are defined as the Stanovoy Mountains, Lake Balkhash, and Caucasus geopotential height indices, respectively. Using these three indices, the effects of the July geopotential height anomalies over the three crucial regions on the 110°–130°E FOPE during the ensuing August were investigated.

The correlation coefficient between the July Stanovoy Mountains geopotential height and August 110°–130°E FOPE indices is 0.35, significant at the 95% confidence

TABLE 1. Correlation coefficients between the August 110°–130°E FOPE and preceding July height indices. Single and double asterisks represent the correlation coefficients higher than the 95% and 99% confidence level, respectively.

Index	Correlation coefficient
Stanovoy Mountains height index	0.35*
Lake Balkhash geopotential height index	0.39*
Caucasus geopotential height index	0.41**
Individual Lake Balkhash geopotential height index	0.19
Lake Balkhash–Caucasus geopotential height index	0.46**

level (Table 1). However, the distribution of correlation coefficients between the July Stanovoy Mountains geopotential height index and the ensuing August geopotential heights shows significant positive correlation over the midlatitude northwestern Pacific, to the east of Japan (Fig. 9a). This region of significant positive correlation (black box in Fig. 9a) is farther east than the region near the Stanovoy Mountains where the 110°–130°E FOPE-related significant positive correlation exists (Fig. 6c). This implies that the July geopotential height anomaly over the Stanovoy Mountains seems to affect the eastern (downstream) geopotential height anomaly rather than the local one during the next month. The regional mean of the August geopotential height to the east of Japan (35°–55°N, 150°–177°E; the black box in Fig. 9a) is not significantly correlated with the simultaneous 110°–130°E FOPE, with a correlation coefficient of −0.10. In addition, the regional mean of the geopotential height to the east of Japan is not significantly correlated with the precipitation over the MLRYR during August (Fig. 9b), with a correlation of −0.11. Given these two nonsignificant relationships, the July Stanovoy Mountains geopotential height index should not be regarded as an important signal that directly contributes to the 110°–130°E FOPE and the associated precipitation anomaly over the MLRYR during August.

The correlation coefficient between the July Lake Balkhash geopotential height and August 110°–130°E FOPE indices is 0.39, significant at the 95% confidence level (Table 1). The correlation between the July Lake Balkhash geopotential height index and simultaneous Z500 (Fig. 10a) shows that a significantly positive correlation extends northeastward from Lake Balkhash to Lake Baikal. During August, the significantly positive correlation continues to extend northeastward and eventually forms a center around the Stanovoy Mountains and the Okhotsk Sea (Fig. 10b), which is where the 110°–130°E FOPE-related key area is located (Fig. 6c).

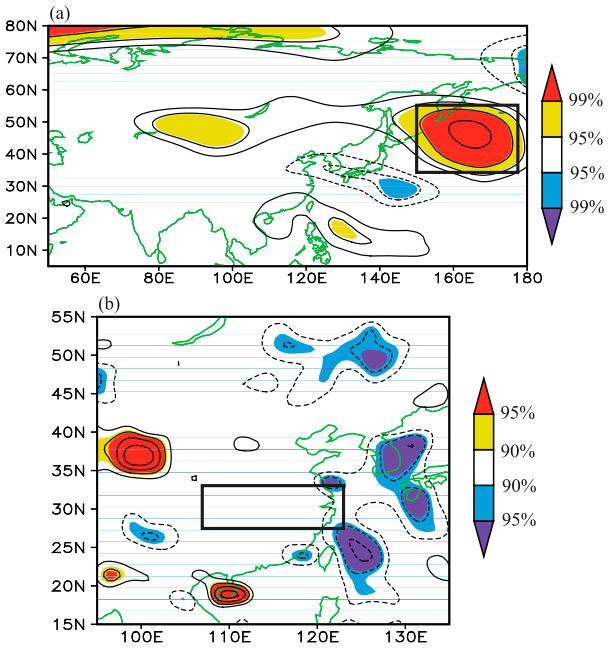

FIG. 9. (a) Distribution of the correlation coefficients between the July Stanovoy Mountains geopotential height index and August 500-hPa geopotential heights during 1979–2017. As shown in the colorbar in (a), yellow (red) shading denotes positive correlations significant at the 95% (99%) confidence level, and blue (purple) shading denotes negative correlations significant at the 95% (99%) confidence level. (b) Distribution of the correlation coefficients between the August regional mean geopotential height to the east of Japan [35°–55°N, 150°–177°E; the black box in (a)] and simultaneous precipitation. The colorbar in (b) denotes the 90% (95%) confidence level. In both (a) and (b), contours are drawn every 0.1 from the beginning contours of ±0.2. The black box in (b) represents the MLRYR region.

The correlation coefficient between the July Caucasus geopotential height index and the August 110°–130°E FOPE is 0.41, significant at the 99% confidence level (Table 1). Figure 11a shows that the geopotential height anomaly over the Caucasus is also remotely correlated with that over Lake Balkhash, generally forming a positive–negative–positive pattern from the Caucasus to Lake Balkhash during July. Similarly, the Lake Balkhash geopotential height anomaly extends northeastward continually, which seems to facilitate the geopotential height anomaly around the Stanovoy Mountains and the Okhotsk Sea during August (Fig. 11b).

The Caucasus geopotential height anomaly is closely connected with the Lake Balkhash geopotential height anomaly during July, with a correlation coefficient of 0.56 (significant at the 99.9% confidence level). Therefore, to examine the individual effect of the Lake Balkhash geopotential height anomaly, we needed to remove the variability of the July Caucasus geopotential height index using the method of linear fitting (Hu et al. 2012).

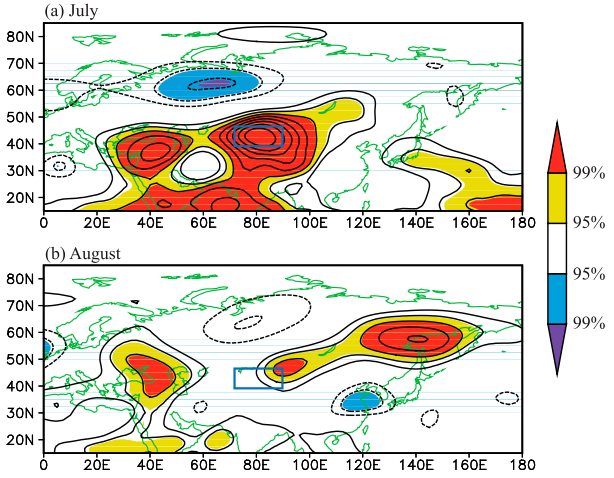

FIG. 10. (a) Distribution of the correlation coefficients between the July Lake Balkhash geopotential height index and simultaneous 500-hPa geopotential heights during 1979–2017. (b) As in (a), but for that between the July Lake Balkhash geopotential height index and August 500-hPa geopotential heights. Contours are drawn every 0.1 from the beginning contours of ±0.2. Yellow (red) shading denotes positive correlations significant at the 95% (99%) confidence level, and blue (purple) shading denotes negative correlations significant at the 95% (99%) confidence level. The blue rectangle represents the Lake Balkhash region.

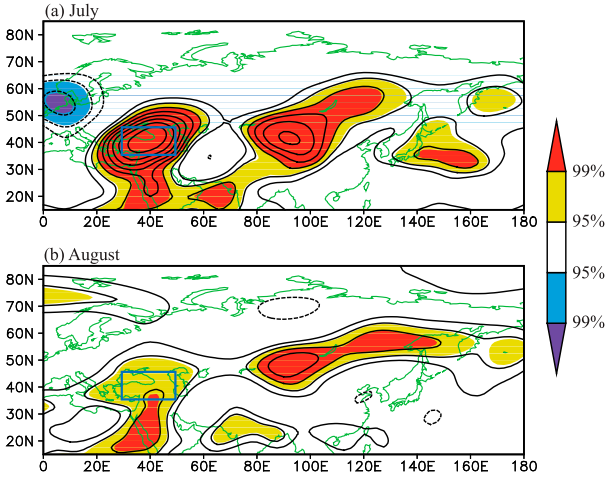

FIG. 11. As in Fig. 10, but for the correlations between the July Caucasus geopotential height index and 500-hPa geopotential heights. The blue boxes represent the Caucasus region.

Figure 12a presents the correlation between the individual Lake Balkhash geopotential height index and Z500 during July. The significant positive correlation over the Balkhash Lake is confined to a local area rather than extending northeastward. Correspondingly, the individual July Lake Balkhash geopotential height index is not significantly correlated with the August 110°–130°E FOPE, with a correlation coefficient of only 0.19 (Table 1). The result implies that the July Lake Balkhash geopotential height anomaly itself is not enough to influence the August 110°–130°E FOPE effectively. Meanwhile, this result also implies that the variation of the July Caucasus geopotential height anomaly can in some way also contribute to that of the August 110°–130°E FOPE.

To further emphasize the combined effect of the Lake Balkhash and Caucasus geopotential height anomalies, a Lake Balkhash–Caucasus geopotential height index was calculated by a simple arithmetic mean of the two indices. The correlation between the July Lake Balkhash–Caucasus geopotential height index and simultaneous (Fig. 12b) and August (Fig. 12c) Z500 clearly shows a relay-like northeastward extension from Lake Balkhash to the Stanovoy Mountains and the Okhotsk Sea via Lake Baikal. As a result, the July Lake Balkhash–Caucasus geopotential height index is closely related to the August 110°–130°E FOPE, with a correlation coefficient of 0.46, significant at the 99% confidence level (Table 1). This correlation coefficient is highest in these preceding geopotential height indices (Table 1).

The combined effect of the July Lake Balkhash and Caucasus geopotential height anomalies on the August geopotential height anomaly around the Stanovoy Mountains and the Okhotsk Sea and the associated August 110°–130°E may be connected with atmospheric slow-varying processes on subseasonal time scales. Correlation analysis revealed that the August 110°–130°E FOPE is also highly correlated with the 1–20 July mean Lake Balkhash–Caucasus geopotential height index, with a correlation coefficient of 0.43, still significant at the 99% confidence level.

Figure 13 shows the correlation between the 1–20 July mean Lake Balkhash–Caucasus geopotential height index and Z500 during different periods on a subseasonal (20-day mean) time scale, which indicates that the Lake Balkhash and Caucasus geopotential height anomalies can persist for a long time from 1–20 July to 1–20 August (Figs. 13a–d). The Lake Balkhash geopotential height anomaly shows a gradual eastward extension from the period 22 July–10 August to the period 12–31 August (Figs. 13c–e). Also, a positive–negative–positive pattern exists from the Caucasus to the Stanovoy Mountains via the Siberian plain during 1–20 August (Fig. 13d).

To further illustrate the daily evolution of the Lake Balkhash and Caucasus geopotential height anomalies on the subseasonal (20-day mean) time scale, a longitude–time Hovmöller diagram along 38°–52°N for the 20-day running mean Z500 anomalies regressed upon the 1–20 July mean Lake Balkhash–Caucasus geopotential height index is presented in Fig. 14. On the 20-day mean time scale, the Lake Balkhash geopotential

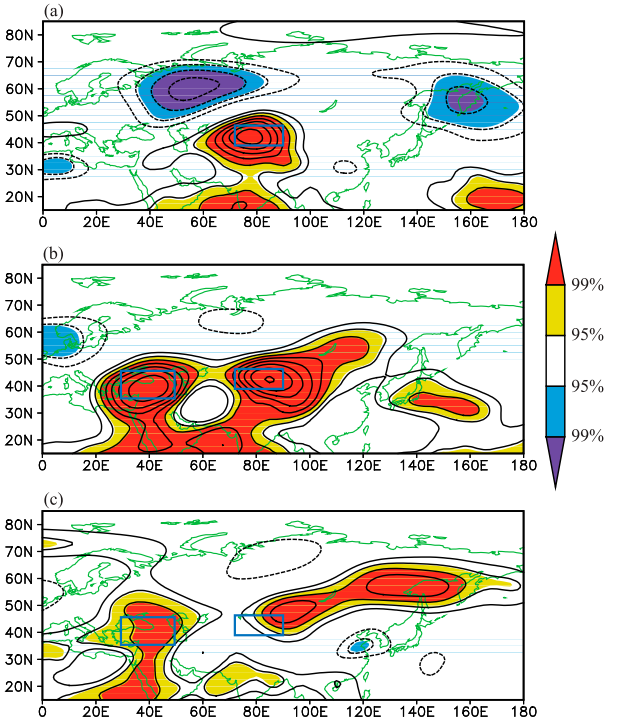

FIG. 12. (a) Correlation of July 500-hPa geopotential heights with the July individual Lake Balkhash geopotential height index after removing the variation of the Caucasus geopotential height index during 1979–2017. (b) As in (a), but for the correlation with the July Lake Balkhash–Caucasus geopotential height index. (c) As in (b), but for the August 500-hPa geopotential heights. Contours are drawn every 0.1 from the beginning contours of ±0.2. Yellow (red) shading denotes positive correlations significant at the 95% (99%) confidence level, and blue (purple) shading indicates negative correlations significant at the 95% (99%) confidence level. The blue box in (a) represents the Lake Balkhash region and the two blue boxes from the left to the right represent the Caucasus and the Lake Balkhash regions in (b) and (c).

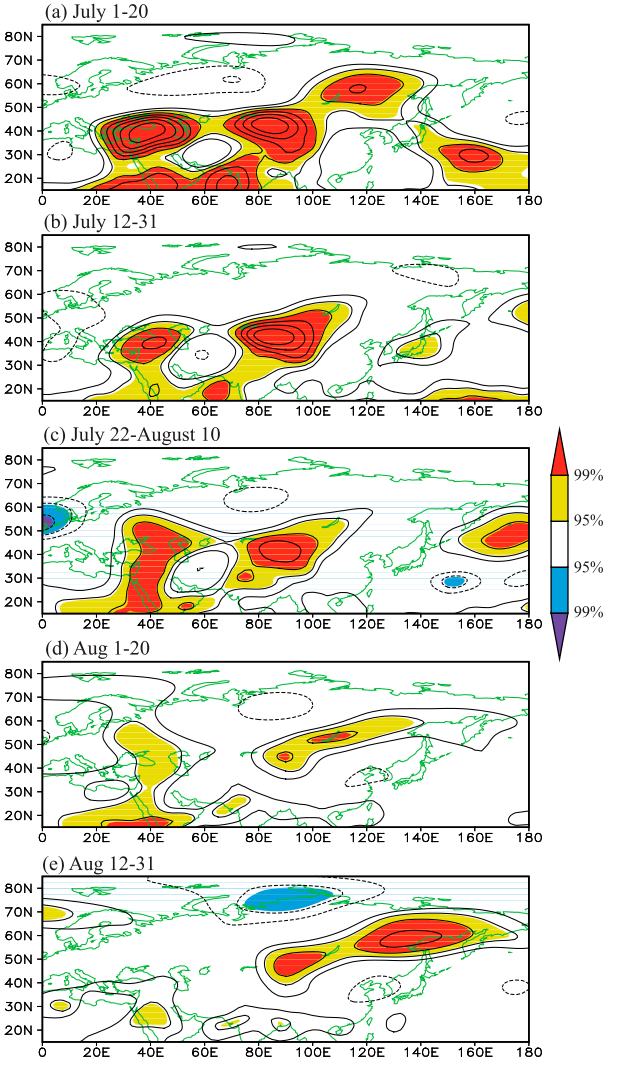

FIG. 13. Correlation between the 1–20 Jul mean Lake Balkhash–Caucasus geopotential height index and 500-hPa geopotential heights on the subseasonal (20-day mean) time scale during different periods: (a) 1–20 Jul; (b) 12–31 Jul; (c) 22 Jul–10 Aug; (d) 1–20 Aug; and (e) 12–31 Aug. Contours are drawn every 0.1 from the beginning contours of ±0.2. Yellow (red) shading denotes positive correlations significant at the 95% (99%) confidence level, and blue (purple) shading indicates negative correlations significant at the 95% (99%) confidence level.

height anomaly around 80°–100°E lasts from the period 1–20 July to the period around 18 July–6 August, and then gradually extends eastward. Finally, it persists and develops around 120°–140°E until 6–25 August. This geopotential height anomaly around 120°–140°E corresponds to the 110°–130°E FOPE-related geopotential height anomaly near the Stanovoy Mountains and the Okhotsk Sea (Fig. 6c). Additionally, the Caucasus geopotential height anomaly around 20°–50°E generally persists from 1–20 July to 1–20 August (Fig. 14). Correspondingly, a positive–negative–positive wave train pattern in geopotential height anomalies forms around 1–20 August (Fig. 14), which seems also to entail the downstream geopotential height anomaly around 120°–140°E, near the Stanovoy Mountains and the Okhotsk Sea. These results imply that the Lake Balkhash and Caucasus geopotential height anomalies play different roles in different periods on the subseasonal time scale.

In summary, the full July (or 1–20 July) mean Lake Balkhash–Caucasus geopotential height index, which reflects the combined effect of the Lake Balkhash and Caucasus geopotential height anomalies, is significantly related to the August geopotential height anomaly around the Stanovoy Mountains and the Okhotsk Sea and the associated August 110°–130°E FOPE. The predictability based on this preceding atmospheric

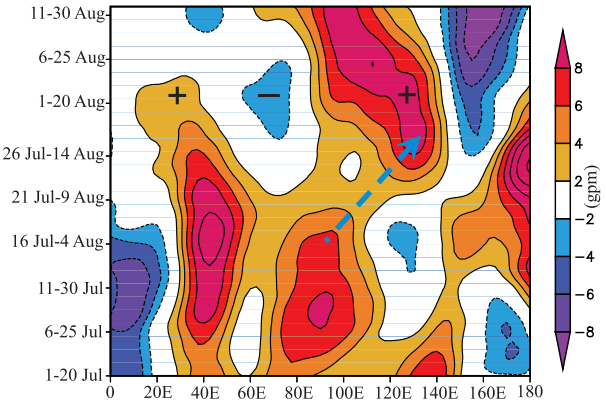

FIG. 14. Longitude–time Hovmöller diagram along 38°–52°N for the 20-day running mean 500-hPa geopotential height anomalies (gpm) regressed upon the 1–20 Jul mean Lake Balkhash–Caucasus geopotential height index. The dashed arrow shows the eastward extension of the geopotential height anomaly from 80°–100°E to 120°–140°E. The +, −, and + indicate a wave train pattern around 1–20 Aug.

signal seems to be linked with slow-varying atmospheric processes on the intraseasonal (20-day mean) time scale. On the subseasonal time scale, the Lake Balkhash and Caucasus geopotential height anomalies might contribute to the geopotential height anomaly around the Stanovoy Mountains and the Okhotsk Sea and the associated August 110°–130°E FOPE, through an eastward extension and through exciting a positive–negative–positive pattern, respectively.

The geopotential height anomaly around the Stanovoy Mountains and the Okhotsk Sea still maintains after the period 12–31 August, when the direct effect of the Caucasus geopotential height anomaly generally disappears (Fig. 13e). This implies that the geopotential height anomaly around the Stanovoy Mountains and the Okhotsk Sea might have another mechanism for its development. Nevertheless, the combined effect of the Lake Balkhash and Caucasus geopotential height anomalies is prior to, and seems also to provide a preceding background for, the development of the geopotential height anomaly around the Stanovoy Mountains and the Okhotsk Sea, which deserves further investigation in the future.

5. Summary and discussion

a. Summary

Based on an approach recently developed by Liu et al. (2018), which can identify and track persistent ridges and blockings as PMZ events effectively, a FOPE was defined to reflect accumulative times/days (i.e., the length of time) when one or multiple PMZ events govern. We explored the relationships between the FOPE over different regions in Eurasia and precipitation over eastern China. The results showed that, of the PMZ events occurring over Eurasia, those over the 110°–130°E region have the closest relationship with the MLRYR precipitation during summer, in particular during August.

The 110°–130°E FOPE is an effective indicator of a longer/shorter duration controlled by the activities of the blockings and ridges near the Okhotsk Sea, and therefore is also linked with the monthly mean anomaly of Z500 near the same region during August. Through the southward Rossby wave energy dispersion of the geopotential height anomaly near the Okhotsk Sea (Shi et al. 2009), the 110°–130°E FOPE is closely related to the mid–high- and midlatitude anomalies of the EAP pattern. Together with the low-latitude anomaly of the EAP pattern, the mid–high- and midlatitude anomalies of the EAP pattern associated with the 110°–130°E FOPE induce a convergence of cold and warm flows and eventually modulate precipitation over the MLRYR.

We also investigated the preceding atmospheric signals of the August 110°–130°E FOPE. The results showed that, on a subseasonal (20-day mean) time scale, the low-frequency signal of the Lake Balkhash geopotential height anomaly can persist and then gradually extend eastward, facilitating the geopotential height anomaly near the Stanovoy Mountains and the Okhotsk Sea and the associated 110°–130°E FOPE. The Caucasus geopotential height anomaly can also last and seems to adjust the downstream geopotential height and the associated 110°–130°E FOPE via the stimulation of a positive–negative–positive pattern. The combined effect of the preceding Lake Balkhash and Caucasus geopotential height anomalies seems to be responsible for, at least partly, the August 110°–130°E FOPE. Moreover, the combined effect may offer a preceding background for the development of the geopotential height anomaly around the Stanovoy Mountains and the Okhotsk Sea itself, although the direct effect will have disappeared. As a result, the full July (or 1–20 July) mean Lake Balkhash–Caucasus geopotential height index, which reflects the combined effect, is significantly correlated with the August 110°–130°E FOPE and should therefore be considered as an important atmospheric predictor. Also, the whole July (1–20 July) mean Lake Balkhash–Caucasus geopotential height index is, to some extent, connected with the August MLRYR precipitation, with a correlation coefficient of 0.27/0.26, approximately at the 90% confidence level. This implies that the preceding Lake Balkhash–Caucasus geopotential height index

can also facilitate the prediction of the August MLRYR precipitation because of its high capability in predicting the August 110°–130°E FOPE.

b. Discussion

Our preliminary results presented here imply that the predictability of the August 110°–130°E FOPE by the preceding Lake Balkhash–Caucasus geopotential height index is possibly due to slow-varying atmospheric processes on the subseasonal (20-day mean) time scale. Stewart (1993) pointed out that the occurrence of a quasi-stationary wave train may induce the formation of a persistent anticyclonic anomaly. Park et al. (2015) found that low-frequency atmospheric motions are responsible for the accelerated mass buildup prior to the peak intensity of a block. These studies implied the possibility that slow-varying atmospheric processes may exert an important impact on blockings, suggesting reasonability in our results. However, several physical mechanisms require further investigation in detail. For instance, the physical process by which the Caucasus geopotential height anomaly excites a positive–negative–positive pattern should be further demonstrated. Also, future research should discuss why the geopotential height anomaly around the Stanovoy Mountains and the Okhotsk Sea can maintain and even develop after the combined effect of the Lake Balkhash–Caucasus geopotential height anomalies disappears. Another key issue is whether and how the slow-varying atmospheric process is modulated by storage and release of thermal signals in underlying surface.

Moreover, some other issues remain unclear, which are also deserving of further exploration in the future. First, besides the definition by Liu et al. (2018), several other methods (e.g., Pelly and Hoskins 2003; Martineau et al. 2017) can also identify nonclosed blockings. We need to further compare the suitability of these methods in studying the variability of the MLRYR precipitation.

Second, the variability of the Lake Balkhash–Caucasus geopotential height index is closely linked with the Silk Road pattern (Lu et al. 2002; Sato and Takahashi 2006; Yasui and Watanabe 2010; Chen and Huang 2012; Hong et al. 2018), which can be clearly identified in the correlation between this index and 200-hPa V winds (not shown). Therefore, it is clearly worth further investigating the relationship between the preceding July Silk Road pattern and the anomalous activities of PMZ events over the 110°–130°E region during August and the associated physical mechanism.

Third, although the July Lake Balkhash–Caucasus geopotential height index is closely related to the August 110°–130°E FOPE, it is not significantly correlated with the August geopotential height over the subtropical northwestern Pacific (i.e., the low-latitude anomaly center of the EAP pattern), with a low correlation coefficient of 0.13. This result indicates that the July Lake Balkhash–Caucasus geopotential height index cannot successfully predict the low-latitude component of the EAP pattern. Therefore, we need to further explore the predictors for the August geopotential height over the subtropical northwestern Pacific. The higher precipitation in summer over the Yangtze River basin is closely linked with winter El Niño events (Xie et al. 2016), which generally results from an enhanced anticyclone (high pressure) over the subtropical northwestern Pacific during the El Niño decaying summer (Wang et al. 2000; Chang et al. 2000). Therefore, from the sea surface temperature anomalies in the tropical Pacific, we may search preceding signals for the low-latitude anomaly center of the EAP pattern. Interestingly, the August 110°–130°E FOPE is not significantly correlated with the tropical Pacific sea surface temperatures during both the preceding winter and spring (not shown). This signifies that, independent of sea surface temperature signals in the tropical Pacific, the August 110°–130°E FOPE and its preceding atmospheric signal are beneficial to, and can therefore be regarded as an important supplement for, the prediction of August MLRYR precipitation. In the future, we will combine the preceding July Lake Balkhash–Caucasus geopotential height index with the preceding tropical Pacific sea surface temperature anomaly to predict the entire anomalous structure of the EAP pattern. The combination of multiple predictors may mean that higher skill can be achieved in predicting the MLRYR precipitation during August.

Acknowledgments. This work was jointly sponsored by the Support Plan of the National Science and Technology (2015BAC03B04), the National Key Research and Development Program of China (Grant 2018YFC1505706), the Strategic Priority Research Program of the Chinese Academy of Sciences (Grant XDA20100300), the National Science Foundation of China (Grant 91637312), the Development Fund of Key Technologies for Meteorological Forecast Operations (Grant YBGJXM2019-04-03), the Research Fund of the Chinese Academy of Meteorological Sciences (Grants 2019KJ022 and 2019Z008), the National Science Foundation of China (Grant 41905091), and the Fund project of National Meteorological Center Forecaster (Grant Y201904). The authors thank the NOAA/OAR/ESRL PSD, Boulder, Colorado, for

providing the NCEP reanalysis and CMAP data from their website at https://www.esrl.noaa.gov/psd/.

REFERENCES

Barnes, E. A., J. Slingo, and T. Woollings, 2012: A methodology for the comparison of blocking climatologies across indices, models and climate scenarios. *Climate Dyn.*, **38**, 2467–2481, https://doi.org/10.1007/s00382-011-1243-6.

Barriopedro, D., R. Garcia-Herrera, A. R. Lupo, and E. Hernandez, 2006: A climatology of Northern Hemisphere blocking. *J. Climate*, **19**, 1042–1063, https://doi.org/10.1175/JCLI3678.1.

Bi, M., and Y. Ding, 1992: A study of budget of potential vorticity of blocking high during the drought period in summer of 1980 (in Chinese). *Quart. J. Appl. Meteor.*, **3**, 145–156.

Black, E., M. Blackburn, G. Harrison, B. Hoskins, and J. Methven, 2004: Factors contributing to the summer 2003 European heatwave. *Weather*, **17**, 4080–4088, https://doi.org/10.1256/wea.74.04.

Brunner, L., G. C. Hegerl, and A. K. Steiner, 2017: Connecting atmospheric blocking to European temperature extremes in spring. *J. Climate*, **30**, 585–594, https://doi.org/10.1175/JCLI-D-16-0518.1.

Bueh, C., and Z. Xie, 2015: An objective technique for detecting large-scale tilted ridges and troughs and its application to an East Asian cold event. *Mon. Wea. Rev.*, **143**, 4765–4783, https://doi.org/10.1175/MWR-D-14-00238.1.

——, N. Shi, L. Ji, J. Wei, and S. Tao, 2008: Features of the EAP events on the medium-range evolution process and the mid- and high-latitude Rossby wave activities during the Meiyu period. *Chin. Sci. Bull.*, **53**, 610–623, https://doi.org/10.1007/s11434-008-0005-2.

Buehler, T., C. C. Raible, and T. F. Stocker, 2011: The relationship of winter season North Atlantic blocking frequencies to extreme cold or dry spells in the ERA-40. *Tellus*, **63A**, 174–187, https://doi.org/10.1111/j.1600-0870.2010.00492.x.

Cattiaus, J., R. Vautard, C. Cassou, P. Yiou, V. Masson-Delmotte, and F. Codron, 2010: Winter 2010 in Europe: A cold extreme in a warming climate. *Geophys. Res. Lett.*, **37**, L20704, https://doi.org/10.1029/2010GL044613.

Chang, C. P., Y. Zhang, and T. Li, 2000: Interannual and interdecadal variation of East Asian summer monsoon and the tropical Pacific SSTs. Part I: Roles of the subtropical ridge. *J. Climate*, **13**, 4310–4325, https://doi.org/10.1175/1520-0442(2000)013<4310:IAIVOT>2.0.CO;2.

Chen, G., and R. Huang, 2012: Excitation mechanisms of the teleconnection patterns affecting the July precipitation in Northwest China. *J. Climate*, **25**, 7834–7851, https://doi.org/10.1175/JCLI-D-11-00684.1.

Chen, L., H. Zong, and Q. Zhang, 2007: The dominant modes of intraseasonal variability of summer monsoon rain belt over eastern China (in Chinese). *J. Atmos. Sci.*, **31**, 1212–1222.

Ding, Y., and G. Hu, 2003: A study on water vapor budget over China during the 1998 severe flood periods. *Acta Meteor. Sin.*, **61**, 129–145.

Dole, R. M., and Coauthors, 2011: Was there a basis for anticipating the 2010 Russian heat wave? *Geophys. Res. Lett.*, **38**, L06702, https://doi.org/10.1029/2010GL046582.

Fan, K., 2006: Atmospheric circulation in Southern Hemisphere and summer rainfall over Yangtze River valley (in Chinese). *Chin. J. Geophys.*, **49**, 599–606, https://doi.org/10.1002/cjg2.873.

Faranda, D., G. Masato, N. Moloney, Y. Sato, F. Daviaud, B. Dubrulle, and P. Yiou, 2016: The switching between zonal and blocked mid-latitude atmospheric circulation: A dynamical system perspective. *Climate Dyn.*, **47**, 1587–1599, https://doi.org/10.1007/s00382-015-2921-6.

Gong, D., J. Yang, S. J. Kim, Y. Gao, D. Guo, T. Zhou, and M. Hu, 2011: Spring Arctic Oscillation-East Asian summer monsoon connection through circulation changes over the western North Pacific. *Climate Dyn.*, **37**, 2199–2216, https://doi.org/10.1007/s00382-011-1041-1.

Gu, W., L. Chen, J. Zuo, and W. Li, 2016: Combined effect of multiple factors on the summer rainfall anomalies over the Huanghe-Huaihe valley in 1992 and 1998 (in Chinese). *Chin. J. Atmos. Sci.*, **40**, 743–755.

Guo, Y., J. Li, and J. Zhu, 2017: A moving updated statistical prediction model for summer rainfall in the middle–lower reaches of the Yangtze River valley. *J. Appl. Meteor. Climatol.*, **56**, 2275–2287, https://doi.org/10.1175/JAMC-D-16-0376.1.

He, B., P. Liu, Y. Zhu, and W. Hu, 2019: Prediction and predictability of Northern Hemisphere persistent maxima of 500-hPa geopotential height eddies in the GEFS. *Climate Dyn.*, **52**, 3773–3789, https://doi.org/10.1007/s00382-018-4347-4.

Hong, X., R. Lu, and S. Li, 2018: Asymmetric relationship between the meridional displacement of the Asian Westerly Jet and the Silk Road Pattern. *Adv. Atmos. Sci.*, **35**, 389–396, https://doi.org/10.1007/s00376-017-6320-2.

Horton, R. M., J. S. Mankin, C. Lesk, E. Coffel, and C. Raymond, 2016: A review of recent advances in research on extreme heat events. *Curr. Climate Change Rep.*, **2**, 242–259, https://doi.org/10.1007/s40641-016-0042-x.

Hoskins, B. J., and T. Woollings, 2015: Persistent extratropical regimes and climate extremes. *Curr. Climate Change Rep.*, **1**, 115–124, https://doi.org/10.1007/s40641-015-0020-8.

Hu, M., D. Gong, L. Wang, T. Zhou, and Z. Zhang, 2012: Possible influence of January-March Arctic Oscillation on the convection of tropical North Pacific and North Atlantic (in Chinese). *Acta Meteor. Sin.*, **70**, 479–491.

Huang, R., and F. Sun, 1992: Impact of tropical western Pacific on the East Asian summer monsoon. *J. Meteor. Soc. Japan*, **70**, 243–256, https://doi.org/10.2151/jmsj1965.70.1B_243.

Kaas, E., and G. Branstator, 1993: The relationship between a zonal index and blocking activity. *J. Atmos. Sci.*, **50**, 3061–3077, https://doi.org/10.1175/1520-0469(1993)050<3061:TRBAZI>2.0.CO;2.

Kalnay, E., and Coauthors, 1996: The NCEP/NCAR 40-Year Reanalysis Project. *Bull. Amer. Meteor. Soc.*, **77**, 437–471, https://doi.org/10.1175/1520-0477(1996)077<0437:TNYRP>2.0.CO;2.

Liu, P., and Coauthors, 2018: Climatology of tracked persistent maxima of 500-hPa geopotential height. *Climate Dyn.*, **51**, 701–717, https://doi.org/10.1007/s00382-017-3950-0.

Lu, R., 2004: Associations among the components of the East Asian summer monsoon system in the meridional direction. *J. Meteor. Soc. Japan*, **82**, 155–165, https://doi.org/10.2151/jmsj.82.155.

——, and R. Huang, 1999: Influence of the stationary disturbance in the Westerlies on the blocking highs over the Northeastern Asia in summer (in Chinese). *Chin. J. Atmos. Sci.*, **23**, 533–542.

——, J. H. Oh, and B. J. Kim, 2002: A teleconnection pattern in upper-level meridional wind over the North African and Eurasian continent in summer. *Tellus*, **54A**, 44–55, https://doi.org/10.1034/j.1600-0870.2002.00248.x.

Martineau, P., G. Chen, and D. A. Burrows, 2017: Wave events: Climatology, trends, and relationship to Northern Hemisphere winter blocking and weather extremes. *J. Climate*, **30**, 5675–5697, https://doi.org/10.1175/JCLI-D-16-0692.1.

Matsueda, M., 2011: Predictability of Euro-Russian blocking in summer of 2010. *Geophys. Res. Lett.*, **38**, L06801, https://doi.org/10.1029/2010GL046557.

Nitta, T., 1987: Convective activities in the tropical western Pacific and their impact on the Northern Hemisphere summer circulation. *J. Meteor. Soc. Japan*, **65**, 373–390, https://doi.org/10.2151/jmsj1965.65.3_373.

Park, T., Y. Deng, W. Li, S. Yang, and M. Cai, 2015: Mass footprints of the North Pacific atmospheric blocking highs. *J. Climate*, **28**, 4941–4949, https://doi.org/10.1175/JCLI-D-14-00598.1.

Parsons, S., J. Renwick, and A. McDonald, 2016: An assessment of future Southern Hemisphere blocking using CMIP5 projections from four GCMs. *J. Climate*, **29**, 7599–7611, https://doi.org/10.1175/JCLI-D-15-0754.1.

Pelly, J. L., and B. J. Hoskins, 2003: A new perspective on blocking. *J. Atmos. Sci.*, **60**, 743–755, https://doi.org/10.1175/1520-0469(2003)060<0743:ANPOB>2.0.CO;2.

Pfahl, S., and H. Wernli, 2012: Quantifying the relevance of atmospheric blocking for co-located temperature extremes in the Northern Hemisphere on (sub-) daily time scales. *Geophys. Res. Lett.*, **39**, L12807, https://doi.org/10.1029/2012GL052261.

Renwick, J., 2005: Persistent positive anomalies in the Southern Hemisphere circulation. *Mon. Wea. Rev.*, **133**, 977–988, https://doi.org/10.1175/MWR2900.1.

Saha, S., S. Moorthi, X. Wu, J. Wang, S. Nadiga, and P. Tripp, 2014: The NCEP Climate Forecast System version 2. *J. Climate*, **27**, 2185–3209, https://doi.org/10.1175/JCLI-D-12-00823.1.

Sato, N., and M. Takahashi, 2006: Dynamical processes related to the appearance of quasi-stationary waves on the subtropical jet in the midsummer Northern Hemisphere. *J. Climate*, **19**, 1531–1544, https://doi.org/10.1175/JCLI3697.1.

Shen, A., G. Ren, and B. Wang, 2008: Analysis and forecasting of relationship between East-Asia Blocking situation and precipitation of China in July (in Chinese). *Climate Environ. Res.*, **13**, 206–211.

Shi, N., C. Bueh, L. Ji, and P. Wang, 2009: Impacts of mid- and high-latitude Rossby wave activities on the medium-range evolution of East Asia/Pacific events during the mid- and late summer (in Chinese). *Chin. J. Atmos. Sci.*, **33**, 1087–1100.

Small, D., E. Atallah, and J. R. Gyakum, 2014: An objectively determined blocking index and its Northern Hemisphere climatology. *J. Climate*, **27**, 2948–2970, https://doi.org/10.1175/JCLI-D-13-00374.1.

Stewart, D. A., 1993: Persistent anomaly forcing in a two-level global circulation model. *J. Atmos. Sci.*, **50**, 2710–2730, https://doi.org/10.1175/1520-0469(1993)050<2710:PAFIAT>2.0.CO;2.

Sun, J., and S. Zhao, 2003: A study of special circulation during Meiyu season of the Yangtze River basin in 1998 (in Chinese). *Climate Environ. Res.*, **8**, 291–306.

Wang, B., R. Wu, and X. Fu, 2000: Pacific–East Asian teleconnection: How does ENSO affect East Asian climate? *J. Climate*, **13**, 1517–1536, https://doi.org/10.1175/1520-0442(2000)013<1517:PEATHD>2.0.CO;2.

——, J. Liu, J. Yang, T. Zhou, and Z. Wu, 2009a: Distinct principal modes of early and late summer rainfall anomalies in East Asia. *J. Climate*, **22**, 3864–3875, https://doi.org/10.1175/2009JCLI2850.1.

——, and Coauthors, 2009b: Advance and prospectus of seasonal prediction: Assessment of the APCC/CliPAS 14-model ensemble retrospective seasonal prediction (1980–2004). *Climate Dyn.*, **33**, 93–117, https://doi.org/10.1007/s00382-008-0460-0.

Wang, Z., and Y. Ding, 2008: Climatic characteristics of rainy seasons in China (in Chinese). *Chin. J. Atmos. Sci.*, **32**, 1–13.

Wu, B., L. Bian, and R. Zhang, 2004: Effects of the winter AO and the Arctic sea ice variations on climate variation over East Asia (in Chinese). *J. Polar Res.*, **16**, 211–220.

Wu, G., H. Liu, F. Chen, and Y. Zhao, 1994: Transient eddy transfer and formation of blocking high on the persistently abnormal weather in the summer of 1980 (in Chinese). *Acta Meteor. Sin.*, **52**, 308–320.

Wu, Z., B. Wang, J. Li, and F. Jin, 2009: An empirical seasonal prediction model of the East Asian summer monsoon using ENSO and NAO. *J. Geophys. Res.*, **114**, D18120, https://doi.org/10.1029/2009JD011733.

Xie, P., and P. A. Arkin, 1997: Global precipitation: A 17-year monthly analysis based on gauge observations, satellite estimates, and numerical model outputs. *Bull. Amer. Meteor. Soc.*, **78**, 2539–2558, https://doi.org/10.1175/1520-0477(1997)078<2539:GPAYMA>2.0.CO;2.

Xie, S., Y. Kosaka, Y. Du, K. M. Hu, J. S. Chowdary, and G. Huang, 2016: Indo-western Pacific ocean capacitor and coherent climate anomalies in post-ENSO summer: A review. *Adv. Atmos. Sci.*, **33**, 411–432, https://doi.org/10.1007/s00376-015-5192-6.

Yasui, S., and M. Watanabe, 2010: Forcing processes of the summertime circumglobal teleconnection pattern in a dry AGCM. *J. Climate*, **23**, 2093–2114, https://doi.org/10.1175/2009JCLI3323.1.

Ye, P., Y. Li, S. Wang, Y. Wang, and K. Shang, 2015: Variation characteristics of different atmospheric blockings and their impact on temperature over the Northern Hemisphere. *J. Lanzhou Univ. Nat. Sci.*, **51**, 639–645.

Yin, H., and C. Li, 2001: Human impact on floods and flood disasters on the Yangtze River. *Geomorphology*, **41**, 105–109, https://doi.org/10.1016/S0169-555X(01)00108-8.

Yu, S., and X. Lin, 2006: Characteristics of two general circulation patterns during floods over the Changjiang Huaihe River Valley (in Chinese). *Acta Meteor. Sin.*, **64**, 605–613.

Zhang, Q., and S. Tao, 1998: Influence of Asian mid-high latitude circulation on East Asian summer rainfall (in Chinese). *Acta Meteor. Sin.*, **56**, 199–211.

——, ——, and S. Zhang, 2001: A study of excessively heavy rainfall in the Songhuajiang-Nenjiang River valley in 1998 (in Chinese). *J. Atmos. Sci.*, **25**, 567–576.

——, C. Xu, Z. Zhang, Y. D. Chen, C. Liu, and H. Lin, 2008: Spatial and temporal variability of precipitation maxima during 1960–2005 in the Yangtze River basin and possible association with large-scale circulation. *J. Hydrol.*, **353**, 215–227, https://doi.org/10.1016/j.jhydrol.2007.11.023.

Zhang, W., H. Li, M. F. Stuecker, F. Jin, and A. G. Turner, 2016a: A new understanding of El Niño's impact over East Asia: Dominance of the ENSO combination mode. *J. Climate*, **29**, 4347–4359, https://doi.org/10.1175/JCLI-D-15-0104.1.

——, and Coauthors, 2016b: Unraveling El Niño's impact on the East Asian Monsoon and Yangtze River summer flooding. *Geophys. Res. Lett.*, **43**, 11 375–11 382, https://doi.org/10.1002/2016GL071190.

Zhao, Z., 1999: *Summertime Droughts and Floods in China and Associated Background Fields* (in Chinese). China Meteorological Press, 279 pp.

Zhou, G., and Q. Zeng, 2001: Predictions of ENSO with a coupled atmosphere–ocean general circulation model. *Adv. Atmos. Sci.*, **18**, 587–603, https://doi.org/10.1007/s00376-001-0047-8.

Zhu, J., G. Zhou, R. Zhang, and Z. Sun, 2013: Improving ENSO prediction in a hybrid coupled model with an em-bedded entrainment temperature parameterisation. *Int. J. Climatol.*, **33**, 343–355, https://doi.org/10.1002/joc.3426.